

**A PROJECT REPORT ON  
THERMAL HYDRAULIC ANALYSIS OF SMALL MODULAR REACTOR (SMR)  
NUCLEAR POWER PLANT**

**SUBMITTED IN  
PARTIAL FULFILLMENT OF THE REQUIREMENT FOR THE AWARD  
OF DEGREE OF**

**BACHELOR OF TECHNOLOGY**

**IN**

**CHEMICAL ENGINEERING**

**SEMESTER- 05**



विद्याधनं सर्वधनं प्रधानम्

**भारतीय प्रौद्योगिकी  
संस्थान जम्मू  
INDIAN INSTITUTE OF  
TECHNOLOGY JAMMU**

**SUBMITTED BY**

**KARAN SHUKLA**

**2022UCH0052**

**SUBMITTED TO**

**INDIAN INSTITUTE OF TECHNOLOGY, JAMMU  
NH-44 , PO NAGROTA, JAGTI, JAMMU AND KASHMIR 181221**

**INDIAN INSTITUTE OF TECHNOLOGY, JAMMU**

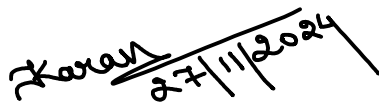
**JAMMU & KASHMIR, INDIA**

**UNDERTAKING BY THE STUDENT**

I **Mr. KARAN SHUKLA** of **B.TECH. (Chemical)** hereby assume that I have followed all the rules and regulations formulated by **Indian Institute of Technology Jammu** regarding project work.

I certify that the Project work entitled represents solely my efforts.

Signature (with date)



.....

(Karan Shukla)

Roll- 2022UCH0052

Indian Institute of Technology Jammu

Jammu and Kashmir, India

**INDIAN INSTITUTE OF TECHNOLOGY, JAMMU**

**JAMMU & KASHMIR, INDIA**

**CERTIFICATE**

This is to certify that, **KARAN SHUKLA , 2022UCH0052** THIRD-year **B-TECH** student of Indian Institute of Technology Jammu has completed his project titled

***“THERMAL HYDRAULIC ANALYSIS OF SMALL MODULAR REACTOR NUCLEAR POWER PLANT”***

This project report may be accepted for evaluation as part of the requirement of B.TECH. (Chemical).

Signature (with date)

---

(Prof. Kannan Iyer)

Signature (with date)

---

(Dr. Yogesh M Nimdeo)

Indian Institute of Technology, Jammu

## **ACKNOWLEDGEMENT**

I express my sincere & heartfelt obligation to **Dr. Yogesh M Nimdeo**, Department of Chemical Engineering, IIT Jammu, Project Supervisor for facilitating me with an opportunity to work on this endeavor. Without his support and cooperation, I would not have made headway in the project.

I am ineffably indebted to **Prof. Kannan Iyer**, Department of Mechanical Engineering, IIT Jammu, Project Co-supervisor for her valuable input, constructive guidance and support, enabling me to complete the project work in its present form.

With deep sense of reverence, I am grateful to God Almighty and my parents who were vital for the success of this project work

**KARAN SHUKLA**

**Roll No. 2022UCH0052**

**IIT JAMMU**

**JAMMU & KASHMIR, INDIA**

## **Abstract:**

This study focuses on the single-channel thermal-hydraulic analysis of fuel assemblies in nuclear power plant and the numerical simulation of control rod (CR) drop dynamics within a guide tube, both essential for nuclear power plant safety analysis.

In a nuclear reactor, heat generation is inherently non-uniform. The heat produced per unit volume is proportional to the number of fission events, which in turn depends on neutron density variations across the reactor. Reactor physicists provide thermal-hydraulic engineers with this critical information on heat distribution. Although exact heat generation calculations are complex, simplified approximations are often applied for practical analysis.

Energy released in fission is distributed among the kinetic energy of fission fragments, kinetic energy of neutrons, and beta, gamma, and neutrino emissions. This energy is released both instantaneously (~90%) and with a delay (~10%). Specifically, 83% of the energy originates from the KE of fission fragments in the fuel, with additional delayed contributions from betas (4%), capture gammas (3%), and fission product gammas (3.5%). Approximately 90% of the total energy remains in the fuel, while the remaining 10% is dispersed in the moderator and structural materials.

The primary goal of thermal-hydraulic analysis is to ensure that critical temperature and heat flux limits are met. Fuel temperature must stay below the allowable limit, typically defined by the metal softening point, while cladding temperature must remain within safe bounds to prevent metal-water reactions. Heat flux must also stay below the Critical Heat Flux (CHF) limit to avoid boiling that could compromise reactor safety.

The drop time of control rod is essential for safety analysis of nuclear power plant. The motion of control rod can be characterized by an annular gap flow with large blockage ratio. In this study, we studied the effects of the control rod drop mechanism. By considering the added mass and the upward flow of fluid in the annular gap, we developed a theoretical model for computing the drop time of concentric control rod.

The mathematical results agree well on the drop time, the histories of velocity and acceleration, and the hydrodynamic characteristics. The present study provides a general method for analysis of control rod drop, which is critical for the nuclear reactor design.

## Content:

CHAPTER No.	TITLE
1	INTRODUCTION
2	TECHNICAL PARAMETERS
3	STEADY STATE THERMAL HYDRAULIC ANALYSIS IN SINGLE CHANNEL
4	THEORETICAL MODEL OF HYDRAULIC CONTROL ROD DRIVEN MECHANISM
5	CONCLUSIONS
6	REFERENCES

# **CHAPTER-1**

## **Introduction**

### **1.1 Single-Channel Thermal-Hydraulic Analysis of Fuel Assemblies**

The performance and safety of nuclear reactors heavily depend on the thermal hydraulic analysis of the reactor core, as it directly influences the reactor's heat distribution, fuel integrity, and coolant flow. One of the most critical aspects of reactor operation is maintaining the temperatures and heat fluxes within safe limits, ensuring the structural integrity of fuel rods and cladding materials. This research focuses on a detailed analysis of the thermal behavior in a nuclear reactor's single-channel, specifically examining the power distribution, temperature profiles, and heat fluxes within the fuel rod assembly. By considering various parameters such as axial and radial power factors, coolant flow characteristics, and fuel rod material properties, this study aims to provide a comprehensive understanding of the heat generation and transfer processes in the core.

Key thermal constraints, including the maximum fuel temperature, cladding temperature, and heat flux limits, are essential to prevent material degradation, hazardous reactions, and boiling phenomena that could threaten reactor safety. The research evaluates the temperature distribution across different reactor components, including the fuel centerline, cladding, and bulk coolant, to identify critical regions that require design optimization. Furthermore, the study integrates a methodology for Single Channel Hot Channel Analysis (HCA), which is used to assess thermal loads and ensure the reactor's safe operation under varying conditions. The results from this analysis are benchmarked against existing data to validate the effectiveness of the applied methodologies and highlight potential areas for improvement in reactor core design and thermal management systems.

### **1.2 Theoretical Model Of Hydraulic Control Rod Driven Mechanism**

Control rods are essential components in nuclear reactors, used to control the neutron flux and, consequently, the reactor's power output. The primary function of a control rod is to absorb neutrons, which regulates the nuclear fission process, allowing for reactor startup, power adjustment, and safe shutdown in both normal and emergency conditions. The control rod drop time is a critical parameter in the design of the control rod drive mechanism

(CRDM), as it determines how quickly the control rod can be inserted into the reactor core to achieve shutdown in the event of an accident, such as a loss of coolant or seismic disturbance.

In many reactor designs, the control rod is positioned concentrically within a guide tube, which allows for a predictable and controlled drop due to gravitational forces. The drop time is influenced by several factors, including the rod's mass, the fluid's viscosity, and the flow dynamics in the guide tube. A rapid drop time is desirable for emergency situations, but it must be balanced with the potential mechanical stresses and impacts that could damage the reactor's components. This trade-off requires careful consideration of the design, including the use of buffer mechanisms to reduce the forces on the fuel assembly and ensure the safe operation of the reactor.

This study focuses on the drop dynamics of a concentrically placed control rod within a guide tube, analyzing the flow characteristics and the associated forces to better understand and optimize the drop time under normal and accident conditions.



# CHAPTER- 2

## Technical Parameters

### Reactor Core Specifications

**Thermal Power Output:** 705 MW (thermal)

#### **Fuel Assemblies:**

- Number of Fuel Assemblies per Core: 55
- Configuration of Fuel Assemblies: Hexagonal
- Assembly Lateral Spacing (W): 234 mm

#### **Fuel Rods:**

- Number of Fuel Rods per Fuel Assembly: 312
- Fuel Rod Length: 3.7 m
- Fuel Rod Outer Diameter (OD): 9.1 mm

#### **Fuel Pellet:**

- Diameter of Fuel Pellet: 7.6 mm

#### **Cladding and Coolant Channel Dimensions:**

- Inner Diameter ( $d_i$ ): 7.73 mm
- Outer Diameter ( $d_o$ ): 9.1 mm

#### **Operating Conditions:**

- Inlet Coolant Temperature: 291°C
- System Pressure: 157 bar

#### **Material Properties:**

- Thermal Conductivity of Cladding Material ( $k_{clad}$ ): 16 W/m·K

# CHAPTER- 3

## Thermal Hydraulic Analysis In Single Channel

### 3.1 Thermal Constraints

The objective of a thermal hydraulic analysis is to ensure that key temperature and heat flux constraints are met to maintain safe reactor operation. First, the maximum fuel temperature must stay within the allowable limit defined by the materials engineer, which is typically based on the metal softening temperature to prevent material degradation. Similarly, the cladding temperature must remain within a safe range to avoid hazardous reactions between the metal and water, which could compromise structural integrity. Additionally, the heat flux should not exceed the Critical Heat Flux (CHF) limit, as surpassing this threshold could lead to boiling and create safety risks. These constraints are fundamental for the reactor's safe and efficient functioning, with further considerations addressed in the context of boiling heat transfer.

### 3.2 Heat Distribution

In bare cylindrical reactors, the spatial variation of neutron flux can typically be represented by a cosine function along the axial direction and a Bessel function of zeroth order in the radial direction. However, in more complex reactor geometries, these spatial distributions become more intricate and challenging to characterize precisely. In such cases, physicists supply the exact shape functions required for analysis. For the purpose of this discussion, we will keep the explanations general to focus on the fundamental concepts, allowing for a broader understanding of spatial variations in reactor cores.

### 3.3 Definitions

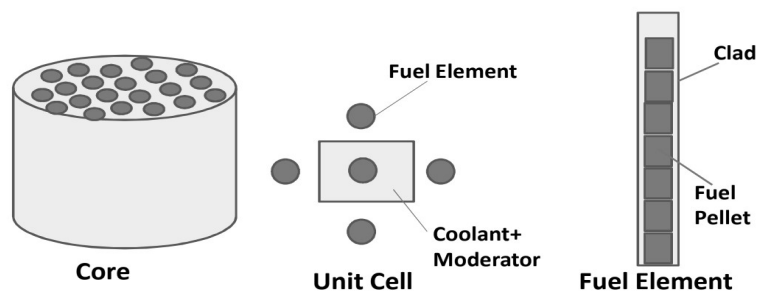


*Figure-3.1: Schematic of reactor core, unit cell, and fuel element design.*

The reactor core is the assembly of the fuel material along with the moderator and coolant material. It can be assumed to be an array of rods distributed in a uniform manner. Each rod consists of an outer cladding and inner fuel pellets. The discussion here considers a square pitch ( $p$ ), which can be straightforwardly extended to any unit cell type. For a unit cell, the volume of the core can be viewed as the total volume of the unit cell. Power density ( $Q'''$ ) is defined as the thermal power generated per unit core volume. Linear heat rate ( $q'$ ) is defined as the thermal power generated per unit length of the fuel rod, and heat flux ( $q''$ ) is the thermal power generated per unit external surface area of the fuel rod.

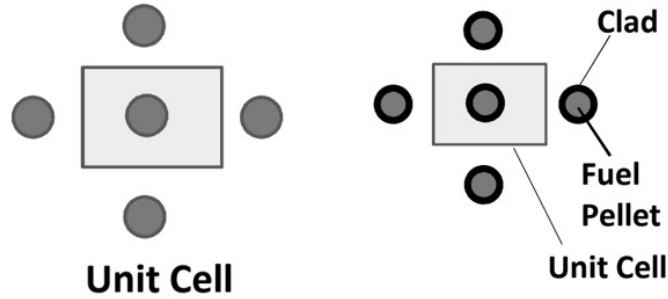


**Figure-3.2 :** Schematic of unit cell , clad, and fuel pellet design.

The volumetric heat generation rate ( $q'''$ ) is defined as the thermal power generated in the core per unit fuel volume. For an infinitesimal control volume ( $dV$ ) within the unit cell, the thermal power generated ( $dQ$ ) can be expressed as the power density ( $q''' = dQ / dV$ ). Similarly, the linear heat rate ( $q'$ ) and heat flux ( $q''$ ) are defined for control volumes of length ( $dl$ ) and external surface area ( $dA$ ), respectively, as expressed in Equations 3.1 to 3.4. Finally, Equation 3.5 highlights the interdependence of these parameters by demonstrating that they differ only by a geometric factor, as  $q'''$ ,  $q'$ , and  $q''$  are all derived from the same  $dQ$ . This relationship enables computation of one parameter from the others based on geometric considerations. Furthermore, since  $dQ$  varies with neutron density, all related parameters exhibit a corresponding dependency.

$$Q''' = \frac{dQ}{p^2 dl} \quad [3.1] \quad q' = \frac{dQ}{dl} \quad [3.2] \quad q'' = \frac{dQ}{\pi d_{rod} dl} \quad [3.3] \quad q''' = \frac{dQ}{\frac{\pi}{4} d_{pellet}^2 dl} \quad [3.4]$$

$$Q''' p^2 = q' = q'' \pi d_{rod} = q''' \frac{\pi}{4} d_{pellet}^2 \quad [3.5]$$

### 3.4 Power Distribution in Nuclear Reactors

To maintain generality in the analysis, a cylindrical reactor is considered, as most power reactors adopt this geometry. However, the approach can be extended to reactors with other shapes. The power distribution is

characterized by radial  $P(r)$  and axial  $P(z)$  power factors as given in Equation 3.6 and 3.7 respectively, which allow the determination of maximum values from average values if  $P(r)$  and  $P(z)$  are known. Using these power factors and geometric considerations, the maximum heat flux, linear heat rate, and volumetric heat generation rates can be computed effectively.

$$P(r) = \frac{1}{\pi R^2} \int_0^R f(r) 2\pi r dr \quad [3.6] \quad P(z) = \frac{1}{H} \int_{-H/2}^{H/2} f(z) dz \quad [3.7]$$

### 3.5 Procedure for Single Channel Hot Channel Analysis in Nuclear Reactors

Single Channel Hot Channel Analysis (HCA) is used to assess nuclear reactor safety. The steps include identifying the hot channel, typically the central fuel channel, which has the highest thermal load. The maximum linear heat rate is calculated by dividing the global average linear heat rate by the product of radial and axial power factors. The mass flow rate for the channel is obtained by dividing the average mass flow rate per channel by a radial factor. Initially, the analysis assumes single-phase, constant-property flow for simplicity, providing a basic estimate of the reactor's thermal-hydraulic behavior.

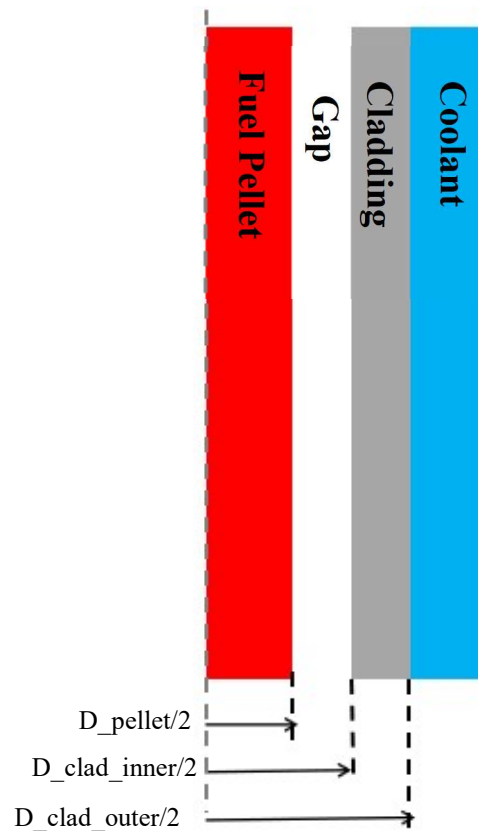


**Figure 3.3 :** The schematic diagram of the Fuel Rod

Energy Balance for an infinitesimal slice at a distance  $z$  can be written as given in Equation 3.8.

$$\dot{m}C_p dT_B = q' \sin\left(\frac{\pi z}{H}\right) dz \quad [3.8]$$

On integration from the entrance to any general point  $z$ , we get Equation 3.9 as given below.

$$\int_{T_{B-in}}^{T_B} dT_B = \frac{q'_{max}}{\dot{m} C_p} \int_0^H \sin\left(\frac{\pi z}{H}\right) dz \quad [3.9]$$

$$T_B = T_{B-in} + \frac{q'_{max} H}{\dot{m} C_p \pi} \left(1 - \cos\left(\frac{\pi z}{H}\right)\right) \quad [3.10]$$

After determining the temperature distribution for the fluid, the next step is to focus on calculating the outer cladding temperature. Using the definition of the convective heat transfer coefficient, the relationship can be expressed as per Equation 3.11.

$$q'' = h(T_{CO} - T_B) \quad [3.11]$$

$$T_{CO}(z) = \frac{q''(z)}{h} + T_B(z) \quad [3.12]$$

To determine the cladding temperature distribution, a conduction analysis must be performed within the cladding material. This involves solving the heat conduction taking into the account thermal properties of the cladding and the boundary conditions imposed by the surrounding fluid and fuel. Therefore after applying the governing equation for axis-symmetric conduction Equation 3.13 is obtained.

$$-\int_{T_C}^{T_{CO}} k_c dT_c = \int_r^{R_{CO}} q'' R_{CO} \frac{dr}{r} \quad [3.13]$$

Assuming thermal conductivity to be constant and taking the limit gives Equation 3.14.

$$T_{CI} = T_{CO} + \frac{q''}{k_c} R_{CO} \ln\left(\frac{R_{CO}}{R_{CI}}\right) \quad [3.14]$$

Before performing conduction analysis in fuel pellet, it is important to calculate pellet outer temperature due to gap between clad and the fuel. The thermal resistance of the gap between fuel and cladding can be reduced by filling it with helium. For conservative estimates, the gap conductance is often assumed to be 5500 W/m<sup>2</sup>-K. The temperature drop across the gap can be estimated using Equation 3.15.

$$\Delta T_{gap} = \frac{q''}{h} \quad [3.15]$$

Thus the fuel surface temperature can be calculated as per Equation 3.16.

$$T_f(R_f) = T_{ci} + \Delta T_{gap} \quad [3.16]$$

Now on perform conduction analysis in fuel pellet and using the boundary condition that  $\frac{dT_f}{dr} = 0$  at centre Equation 3.17 is obtained as follow.

$$\int_0^{T_f(0)} k_f dT_f - \int_0^{T_f(R_f)} k_f dT_f = \frac{q'}{4\pi} R_f^2 \quad [3.18]$$

The integral  $\int k dT$ , derived from Westinghouse Composite K, is closely aligned with Lyon's equation when considering 95% theoretical density. This approach is detailed in the works of Kazimi and Todreas. Figure 3.1 3.19 is used to calculate  $\int k dT$ .

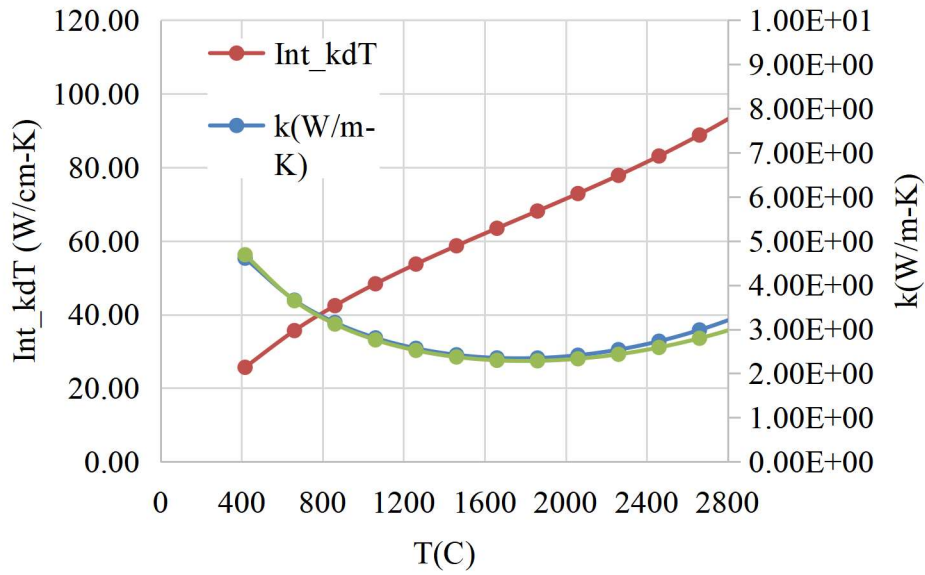


**Figure 3.4:**  $\int k dT$  is plotted against  $T$

### 3.6 Calculation Procedure

- 1) Axially divide the entire fuel rod into certain number of elemental sections.
- 2) Evaluate bulk temperature, outer clad temperature, inner clad temperature and pellet surface temperature.
- 3) Assume certain fuel centre-line temperature and calculate  $\int_0^{T_f(0)} k_f dT_f$  and  $\int_0^{T_f(R_f)} k_f dT_f$  using figure 3.4 .
- 4) Calculate difference of both the integrals calculated in point '3' and then find  $\frac{q'}{4\pi}$
- 5) Take absolute error of both and goal seek to zero.
- 6) This will find the fuel center-line temperature.

Note that it is important to design the material of clad and fuel pins within the maximum temperature limits. The calculation has been performed in EXCEL and the calculation table s reported in table 3.1.

S.No	Parameters	Values
1	Power per rod (kW)	41
2	Side of triangle (mm)	135.1
3	Hexagonal Cross Section( $m^2$ )	0.047
4	Flow Area per Hexagon( $m^2$ )	0.027
5	Coolant Flow area in Core( $m^2$ )	1.49
6	Volumetric Flow of Coolant in core( $m^3$ )	5.61
7	Average Velocity of coolant in core (m/s)	3.76
8	Average Linear Heat rate(kW/m)	11.1
9	Hydraulic Diameter (mm)	11.15
10	Re	362332
11	Pr	0.84
12	Nu	601
13	Radial peaking factor	2.32
14	$q'_{av}$ (W/m)	11103.7611
15	$q'_{avg, central channel}$ (W/m)	25760.72576
16	Axial Peaking Factor	1.570796327
17	$q'_{max, central channel}$ (W/m)	40464.85341
18	$\dot{m}$ /Rod(kg/s)	0.243609379
19	Orificed $\dot{m}$ (kg/s)	0.565173759

**Table 3.1** : The calculated data for single channel is shown

### 3.7 Results and Discussion

The inlet coolant temperature is 291°C, and the outlet coolant temperature for the given SMR is 321°C. Through our study, we are benchmarking the same outlet temperature, which validates the methodology applied for studying the single-channel analysis. At the inlet and outlet of the core, the bulk coolant temperature, clad outer temperature, and fuel centerline temperature are identical.

Figure 3.5 clearly shows that the temperature rises up to a certain point and then decreases, exhibiting sinusoidal behavior for the outer clad temperature and the fuel centerline temperature. However, for the bulk coolant temperature, it increases monotonically and reaches 321.06°C at the core outlet.

At all the axial locations the fuel centerline temperature is the highest, followed by the outer clad temperature, and then the bulk coolant temperature. This is because the fission reaction generates the highest amount of heat at the fuel centerline. The maximum outer clad temperature is 346°C, while the maximum fuel centerline temperature is 1857.22°C.

Therefore, it is essential to select a fuel rod material with a melting or softening temperature higher than these values to prevent the material from melting.

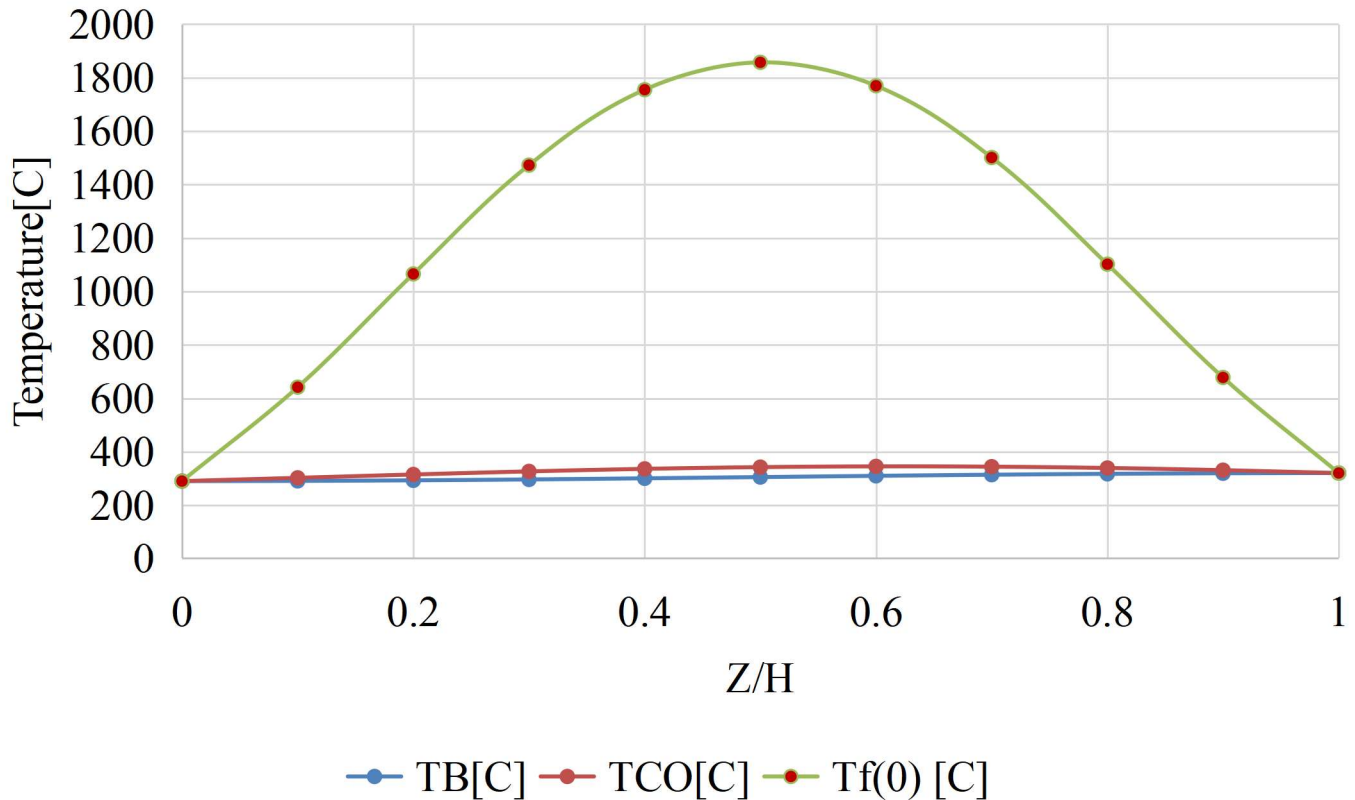


**Figure 3.5:** Graph representing the fuel centerline temperature ( $T_f(0)$ ), outer clad temperature ( $T_{CO}$ ), and bulk coolant temperature ( $T_B$ ).



# CHAPTER - 4

## Theoretical Model Of Hydraulic Control Rod Driven Mechanism (CRDM)

In various control rod cases, the CRDM encompasses different configurations of flow channels. This study primarily focuses on the rod drop scenario in water reactor control rods, analyzing a single-channel configuration. A single channel refers to a setup where the fluid flows exclusively through one pathway—the annular space between the control rod and the guide tube. As the control rod drops, a portion of the fluid is displaced upwards through the annular gap, creating a jet-like flow. Figure 4.1 illustrates a schematic representation of the concentric rod drop. The blockage ratio ( $\alpha$ ) is defined as the proportion of the control rod's outer diameter ( $r$ ) to the guide tube's inner diameter ( $R$ ), expressed as  $\alpha = r/R$ .

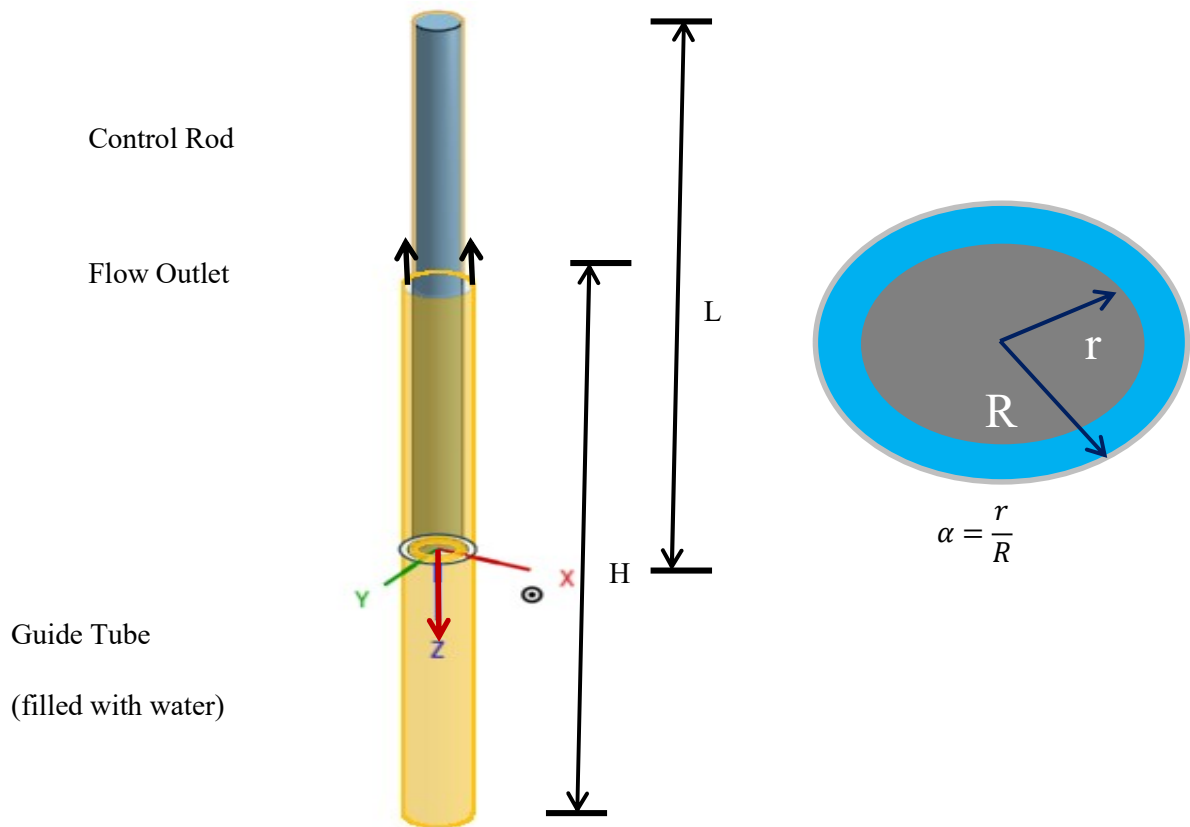


Figure 4.1 : Schematic diagram of concentric rod drop. The area shaded with blue color represents the fluid domain.

#### 4.1 Governing equation of Control rod drop

When a control rod drops in a viscous fluid, it is subjected to several forces, including gravity, buoyancy, fluid forces caused by added mass, viscous friction drag, and pressure drag. The motion of the control rod is described by the equation of motion:

$$G - F_B - F_a - F_f - F_p = m \frac{d^2 z}{dt^2} \quad [4.1]$$

In this equation,  $G$  represents the gravitational force acting on the control rod,  $F_B$  is the buoyant force,  $F_a$  denotes the inertial force of the fluid due to added mass,  $F_f$  corresponds to the viscous friction drag, and  $F_p$  is the pressure drag. Here,  $m$  is the total mass of the control rod,  $z$  is the displacement of the control rod during its drop, and  $t$  is the drop time. This relationship captures the dynamic balance of forces governing the control rod's movement through the viscous medium.

#### 4.2 Force analysis

##### (1) Gravity

Gravity is the force exerted on the control rod by the attraction of the earth, which is proportional to the acceleration of gravity, i.e.

$$G = mg \quad [4.2]$$

in which  $g$  is the gravitational acceleration.

##### (2) Buoyancy

Buoyancy is caused by the difference in hydrostatic pressure on the surface of an object immersed in a fluid:

$$F_B = \rho V_B g \quad [4.3]$$

in which  $\rho$  is the density of the fluid (water),  $V_B$  is the volume of control rod immersed in fluid and can be calculated as follows:

$$V_B = z A_{rea} \quad [4.4]$$

in which Area is the cross-sectional area of control rod, i.e.,  $\text{Area} = \pi r^2$ .

### ***(3) Fluid inertia force***

When the control rod drops in an unsteady state in the fluid, the inertial force exerted by the fluid on the control rod is equivalent to the inertial force generated by a mass attached to the mass of the control rod i.e.

$$F_a = m' \frac{d^2 z}{dt^2} \quad [4.5]$$

in which  $m'$  is the added mass. It should be noted that the direction of the inertial force of the fluid is opposite to the direction of the control rod's acceleration. The added mass can usually be expressed in the following form

$$m' = k\rho V_B \quad [4.6]$$

in which  $k$  is the added mass coefficient. For fluids in an infinite domain, the added mass coefficient is typically taken as 1.0. However, in the case of annular gap flow, where the outer diameter is  $R$  and the inner diameter is  $r$ , the added mass coefficient  $k$  is influenced by the blockage ratio  $\alpha$ . Chung and Chen (1977) proposed an analytical approach based on two-dimensional potential flow theory to assess the hydrodynamic masses of multiple circular cylinders submerged in a fluid within a cylindrical container. For a concentrically positioned control rod, the added mass can be determined using the following equation:

$$k = \frac{R^2 + r^2}{R^2 - r^2} = \frac{1 + \alpha^2}{1 - \alpha^2} \quad [4.7]$$

When  $R \gg r$ , the blockage ratio  $\alpha$  approaches zero, which is equivalent to the case of fluid in an infinite domain, where the added mass coefficient  $k$  equals 1.0. Additionally, as shown in Equation 7, the added mass coefficient increases with the increase in the blockage ratio. Figure 4.2 illustrates how the added mass coefficient varies with the blockage ratio for a concentrically positioned control rod.

### ***(4) Viscous friction drag***

The wall viscous friction drag acting on a control rod in an annular channel arises due to the boundary layer effects of the viscous fluid, generating shear stress on the wetted surface. To calculate this drag, the formula commonly used for circular tubes can be adapted by replacing the tube diameter with the equivalent diameter of the annular channel. The resulting expression incorporates the dimensionless viscous friction coefficient ( $f$ ), the contact length

( $l$ ) between the control rod and the fluid (equal to the control rod's drop displacement,  $z$ , in this case), the equivalent diameter of the annular channel ( $D_E$ ), and the relative velocity ( $v$ ) between the control rod and the fluid.

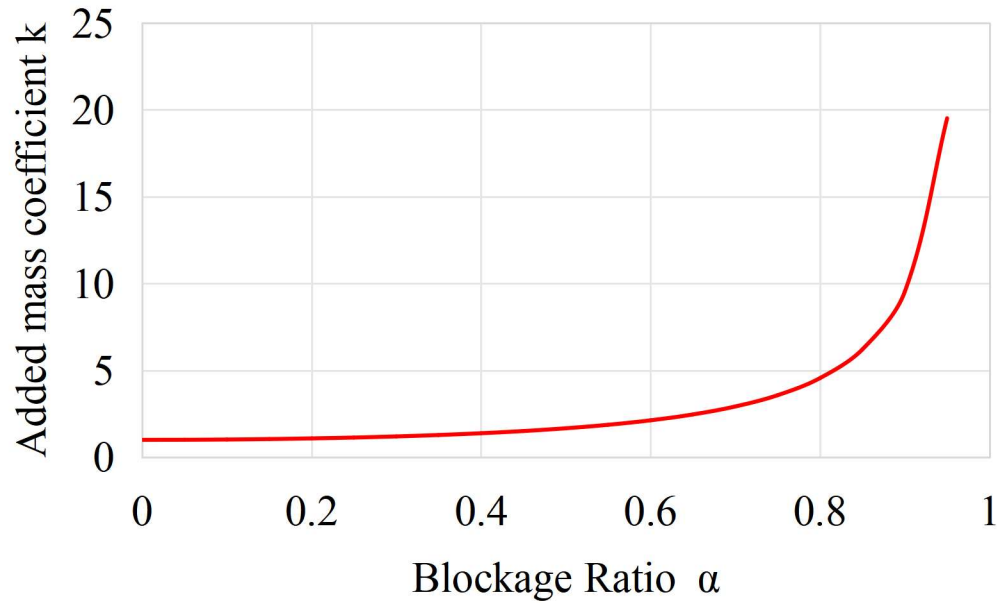


Figure 4.2 : Added mass coefficient as function of blockage ratio for concentrically located control rod.

$$F_f = f \frac{l}{D_E} \frac{1}{2} \rho v^2 A_{rea} \quad [4.8]$$

The equivalent diameter  $D_E$  can be calculated by the following formula:

$$D_E = R - r \quad [4.9]$$

The dimensionless viscous friction coefficient  $f$  is related to parameters such as Reynolds number and wall roughness. For laminar flow,  $f$  can be calculated by the following formula:

$$f = \frac{64}{Re} \quad [4.10]$$

and for turbulent flow,  $f$  can be calculated with (Wang et al., 1994):

$$f = C_t Re^{-0.25} \quad [4.11]$$

$$C_t/C_{t0} = \sqrt[3]{0.0154 \frac{C_i}{C_{i0}} - 0.012 + 0.85} \quad [4.12]$$

in which  $C_{t0}$  is the turbulent geometric parameter of a circular pipe,  $C_{t0}=0.3164$  in hydraulically smooth areas;  $C_t$  is the turbulent geometric parameter for non-circular pipes;  $C_i$  and  $C_{i0}$  are laminar flow geometric parameters for non-circular and circular pipes, respectively. In this study,  $C_t$  can be taken as 0.3395 according to the size ratio of the actual control rod drive line.

Re is the Reynolds number and defined as follows:

$$Re = \frac{v D_E}{\vartheta} \quad [4.13]$$

in which  $\vartheta$  is the kinematic viscosity of fluid. The relative velocity  $v$  between the control rod and the fluid is the velocity at which the control rod drops plus the velocity at which the fluid flows upward, i.e

$$v = \frac{dy}{dt} + v_w \quad [4.14]$$

in which  $v_w$  is the upward annular gap flow velocity of fluid. In the present study, we can first calculate an average velocity of upward flow of the fluid through flow conservation as following:

$$v_w = \frac{r^2}{R^2 - r^2} \frac{dz}{dt} \quad [4.15]$$

## (5) Pressure drag

Pressure drag on the control rod arises from flow separation at its trailing edge, which is caused by viscosity, and the pressure difference between the tail and head of the rod (dynamic differential pressure). This drag can be calculated using the following formula:

$$F_p = C_D \frac{1}{2} \rho v^2 A_{rea} \quad [4.16]$$

where  $C_D$  is the drag coefficient, and it depends on factors such as the Reynolds number and the length-to-diameter ratio of the control rod. For different flow regimes, the drag coefficient behaves as follows:

$$C_D = \begin{cases} 64/Re, & Re \ll 1 \\ 1.2, & 10^3 < Re < 10^5 \end{cases} \quad [4.17]$$

The final governing equation of eccentric rod drop can be obtained by substituting the above force components into Eq. (1):

$$mg - \rho y A_{rea} g - m' \frac{d^2 z}{dt^2} - f \frac{z}{D_E} \frac{1}{2} \rho \left( \frac{dz}{dt} + v_w \right)^2 A_{rea} - C_D \frac{1}{2} \rho \left( \frac{dz}{dt} + v_w \right)^2 A_{rea} = m \frac{d^2 z}{dt^2} \quad [4.18]$$

with the initial conditions:

$$\begin{cases} \left. \frac{dz}{dt} \right|_{t=0} = 0 \\ \left. \frac{d^2 z}{dt^2} \right|_{t=0} = g \end{cases} \quad [4.19]$$

By solving this second-order variable coefficient nonlinear ordinary differential equation, the displacement time histories, velocities, accelerations, and hydrodynamic characteristics of the control rod can be obtained.

### 4.3 Calculation Conditions

<i>Parameter</i>	<i>Symbol</i>	<i>Value</i>	<i>Unit</i>
Gravitational acceleration	g	9.81	m/s <sup>2</sup>
Density of water	ρ	998	kg/m <sup>3</sup>
Kinematic viscosity of water	ν	1.003×10 <sup>-6</sup>	m <sup>2</sup> /s
Radius of guide tube	R	0.1	meters
Radius of control rod	r	0.05	meters
Density of control rod	ρ <sub>CR</sub>	1200	kg/m <sup>3</sup>
Length of control rod	H	1.6	meters
Length of guide tube	L	1.25	meters

Table 4.1: Geometrical dimensions and physical properties of the fluid Used in the code.

## 4.4 Results and Discussion

In this section, the results obtained from the numerical code simulating the dynamics of the control rod are presented and discussed. The code computes the motion of the control rod under the influence of forces such as buoyant force, inertial force, viscous frictional drag and pressure drag. The primary outputs of the code include displacement, velocity, and the forces acting on the control rod over time and position.

### 4.4.1 The relationship between displacement and time

Figure 4.3 illustrates the displacement-time relationship for a control rod descending in a guide tube, with a total drop time of 0.651 seconds and a terminal velocity of 2.22 m/s. Initially, the rod starts from rest, and the curve's increasing slope indicates acceleration as gravitational force dominates over resistive forces such as viscous drag and pressure drag. However, as the rod accelerates, these resistive forces increase proportionally with velocity, gradually countering the gravitational driving force.

The velocity curve's slope decreases over time, indicating a reduction in acceleration as the rod approaches its terminal phase. Near the end of the descent, the resistive forces equal and eventually exceed the gravitational force, causing the acceleration to become negative. This results in a tapering displacement curve as the rod decelerates slightly before reaching the bottom. The shift from positive to negative acceleration highlights the dynamic balance between driving and resistive forces during the rod's descent.

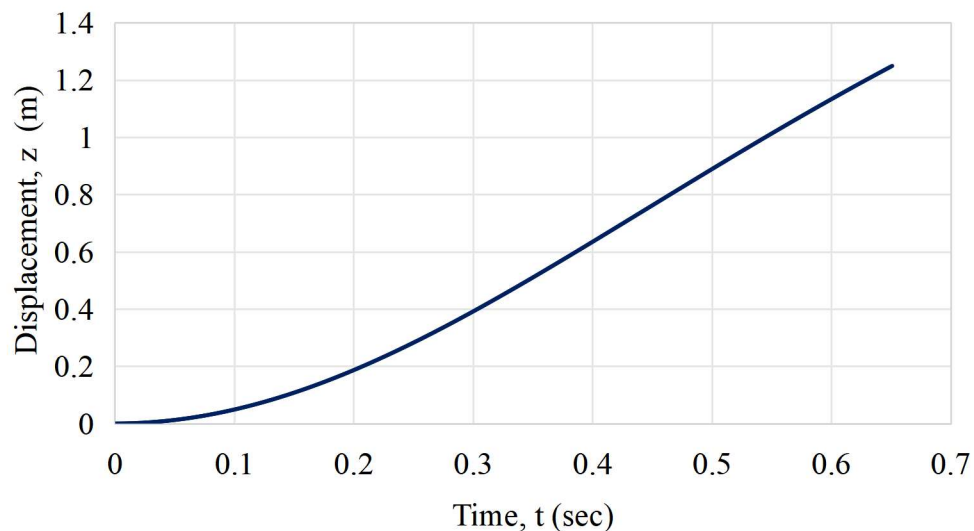


*Figure 4.3: Displacement of the Control Rod (CR) as a function of time.*

#### **4.4.2 The relationship between velocity and time**

Figure 4.4 illustrates the velocity-time relationship for the control rod as it descends through the guide tube. The velocity initially increases, reaching a peak of 2.55 m/s at 0.445 seconds. Beyond this point, the velocity begins to decrease, ultimately reducing to 2.22 m/s as the rod completes its descent in 0.651 seconds. The decreasing slope of the velocity curve signifies a continuous reduction in acceleration throughout the drop.

Initially, the gravitational force dominates, driving the rod's acceleration. However, as the rod's velocity increases, resistive forces such as viscous drag, pressure drag, and buoyancy become more significant. After 0.445 seconds, these resistive forces surpass the gravitational force, resulting in deceleration. The acceleration at 0.445 seconds is calculated as  $0.00676 \text{ m/s}^2$ . Upon reaching the bottom, the net upward acceleration acting on the rod is  $2.66 \text{ m/s}^2$ , indicating the dominance of resistive forces over gravity. This analysis highlights the critical balance of forces influencing the rod's motion and provides insights into the dynamics of its descent.

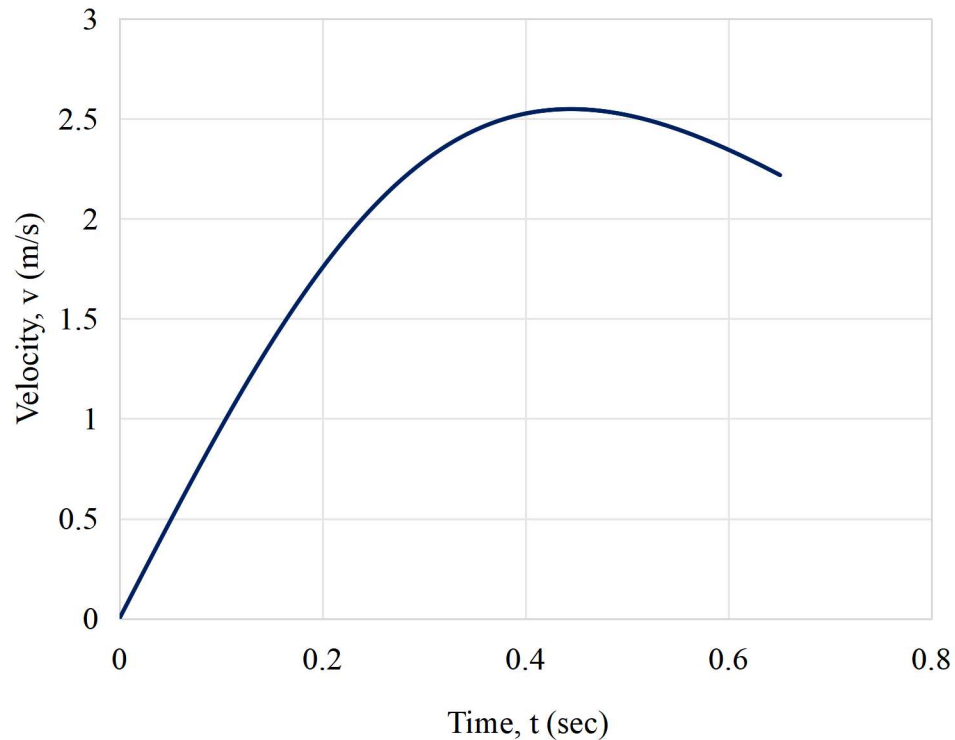


*Figure 4.4: Velocity of the Control Rod (CR) as a function of time.*



### 4.4.3 Time Step Independence Test

To ensure the accuracy of the numerical results obtained from the code, a time step independence test was performed. Different time step values were evaluated by running the code with varying time intervals and comparing the results of displacement, velocity, and force. The results showed that as the time step decreased, the computed displacement and velocity curves converged, indicating that the time step chosen for the final calculations (i.e.,  $\Delta t = 0.001 \text{ s}$ ) is sufficient to minimize numerical errors. This confirms that the selected time step is appropriate for capturing the dynamics of the control rod accurately. Table 4.2 shows the drop time for different time steps.

S.No.	$\Delta t$ (s)	Drop time (s)
1	0.001	0.651
2	0.005	0.645
3	0.01	0.640

*Table 4.2: Time-step independence test showing the effect of varying time steps on results.*

### 4.4.4 Forces acting on Control Rod

Figures 4.5 and 4.6 illustrate the forces acting on the control rod during its downward motion in the guide tube, focusing on buoyant, pressure drag, and viscous drag forces. The buoyant force increases over time as more water is displaced from the annular region between the rod and the guide tube, reaching a peak value of 96.04 N by the end of the simulation. This rise in buoyant force is due to the increasing volume of displaced water as the rod moves downward.

The pressure drag force initially increases with velocity but later decreases as the rod decelerates after 0.445 seconds. This reflects the dynamic balance between the rod's speed and the fluid resistance.

The viscous drag force remains steady, ranging from 0–20 N, gradually increasing as the rod moves downward and more fluid is displaced. Initially, the pressure drag force dominates, but after 0.71 seconds, the buoyant force surpasses it, becoming the primary resistive force acting on the rod.

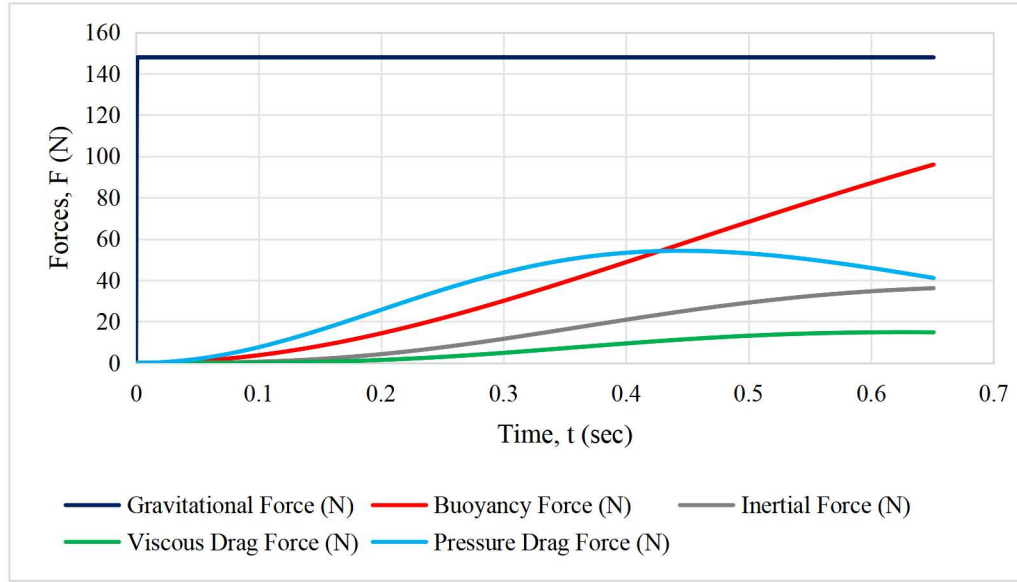


Table 4.5: Forces acting on Control Rod against time is shown.

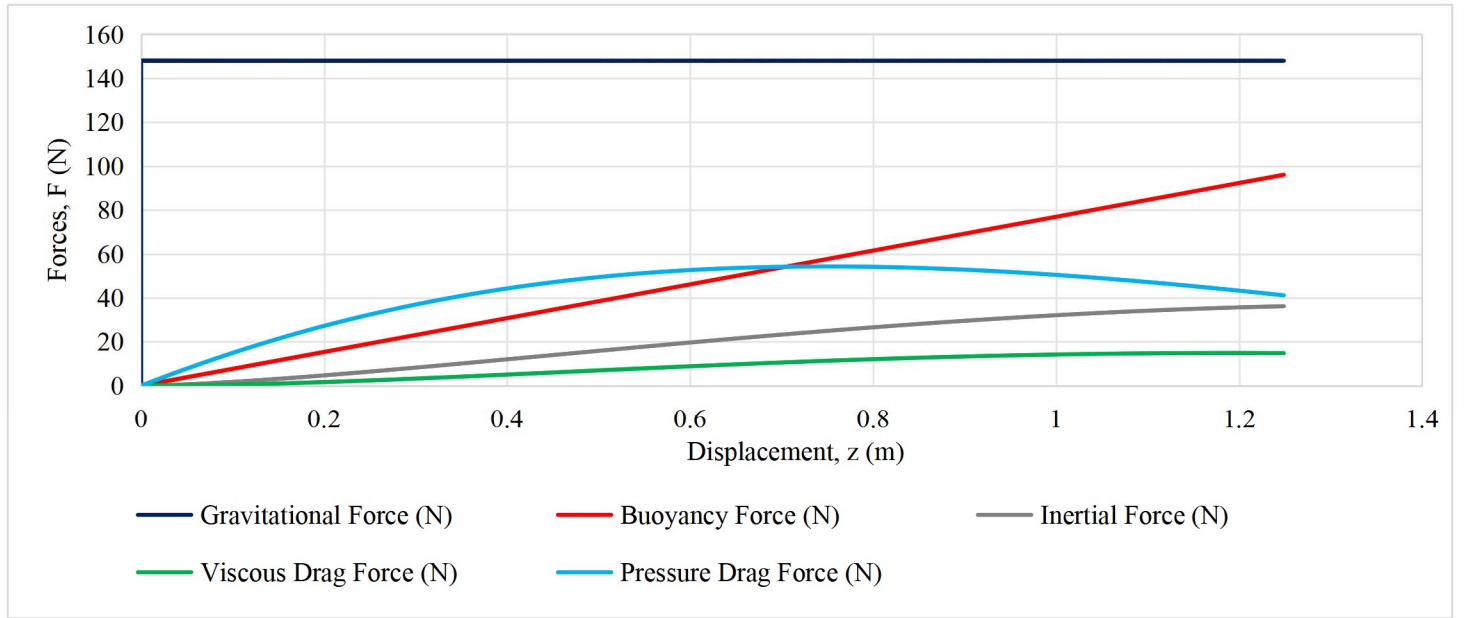


Table 4.6: Forces acting on Control Rod against its displacement is shown.

#### 4.4.5 Verification of Results

The net force at each time step can be determined using two fundamental approaches. The first involves (*Net Force-1*) applying Equation 4.1, while the second relies (*Net Force-2*) on the derivative of velocity to compute acceleration. Multiplying the acceleration by the mass of the control rod yields the net force.

To validate the results, the forces acting on the system were calculated separately using distinct functions in the code. The net force was then obtained using the second approach (via acceleration). Subsequently, the net force was independently calculated using Equation 4.1 and cross-checked against the values derived from the second approach. The comparison showed negligible error, indicating the correctness of the methodology employed to solve the problem. It is noted, however, that certain factors were not considered in this analysis, such as ground excitation effects and deformation of the control rod. These omitted factors, including the contact and friction between the control rod and the guide tube, may influence the results in scenarios involving varied control rod drop states. These simplifications were deliberate to streamline the scope of the discussion and the net force equation.

The average error was calculated to be 0.289 N, determined by taking the average of the absolute differences between the net force values obtained through the two approaches at each time step. Mathematically, this can be expressed as:

$$\text{Average Error} = \frac{1}{N} \sum_{i=1}^N |(\text{Net Force} - 2) - (\text{Net Force} - 1)| \quad [4.20]$$

where Net Force-2 and Net Force-1 represent the net forces calculated using the second approach (via acceleration) and Equation 4.1, respectively, and N is the total number of time steps.

# CHAPTER - 5

## Conclusions

### *5.1 Steady State Thermal Hydraulic Analysis In Single Channel*

The results from the single-channel thermal analysis of the SMR core reveal several critical insights into the temperature distribution within the fuel rod, its cladding, and the surrounding coolant. The following conclusions can be drawn from this study:

1. **Temperature Distribution:** The fuel centerline temperature is the highest among the various thermal profiles, reaching up to  $1857.22^{\circ}\text{C}$ , followed by the outer cladding and bulk coolant temperatures. This behavior is due to the higher heat generation at the fuel centerline from fission reactions.
2. **Coolant and Cladding Behavior:** The bulk coolant temperature increases monotonically, reaching a stable outlet temperature of  $321.06^{\circ}\text{C}$ , while the outer cladding temperature exhibits a sinusoidal pattern, reflecting the interaction between heat generation and heat transfer dynamics.
3. **Material Selection:** The maximum fuel centerline temperature underscores the necessity of selecting fuel and cladding materials with higher melting or softening points to ensure structural integrity and prevent material failure during operation.
4. **Validation of Methodology:** The study's results validate the thermal analysis methodology, as the outlet temperature of the coolant aligns with expected values, confirming the accuracy and reliability of the computational approach used.
5. **Design Considerations:** These findings emphasize the importance of designing reactor components, particularly the fuel rod and coolant system, with temperature limits in mind to ensure safe and efficient reactor operation.

This research provides valuable data for improving reactor design, ensuring thermal management, and advancing safety protocols in nuclear systems.

### *5.2 Theoretical Model Of Hydraulic Control Rod Driven Mechanism (CRDM)*

1. The numerical simulations effectively modeled the control rod's dynamics, offering a comprehensive understanding of the forces involved in its descent, including buoyant force, gravitational force, and resistive forces like viscous and pressure drag.
2. The displacement-time and velocity-time curves highlight the key phases of the rod's motion: initial acceleration driven by gravity, followed by deceleration as resistive forces, particularly buoyancy and drag, become more significant with increasing velocity.

3. A critical observation is that buoyant force increases steadily with the rod's displacement, ultimately surpassing pressure drag after 0.71 seconds and dominating as the primary resistive force by the end of the descent, significantly influencing the rod's deceleration.
4. The time-step independence test demonstrated the robustness of the simulation, confirming the accuracy and reliability of the results, with minimal numerical error in displacement and velocity calculations.
5. While simplifications such as neglecting ground excitation and contact forces were made, the findings validate the computational methodology, underscoring its potential for modeling complex control rod dynamics with high precision in similar nuclear reactor scenarios.

# CHAPTER - 6

## References

1. Arthur EM, Zhang C, Debrah SK, Yamoah S, Wang L. Numerical simulation for the control rod assembly drop time evaluation in a LFR. *Heliyon*. 2022 Nov 9;8(11):e11540. doi: 10.1016/j.heliyon.2022.e11540. PMID: 36406737; PMCID: PMC9672312.
2. Babkin, V.A. Couette Longitudinal Turbulent Flow Between Coaxial Cylinders. *J Eng Phys Thermophy* 87, 184–190 (2014). <https://doi.org/10.1007/s10891-014-0998-0>
3. Zhao, P., Liu, Z., Yu, T., Xie, J., Chen, Z., & Shen, C. (2020). Code development on steady-state thermal-hydraulic for small modular natural circulation lead-based fast reactor. *Annals of Nuclear Energy*, 141, 107010. <https://doi.org/10.1016/j.anucene.2020.107010>
4. Kim, JaeYong, KyungHo Yoon, Se-Hong Oh, and SungHo Ko. "CFD analysis to estimate drop time and impact velocity of a control rod assembly in the sodium cooled faster reactor." *The KSFM Journal of Fluid Machinery* 18, no. 6 (2015): 5-11.
5. <https://www.energy.gov/ne/advanced-small-modular-reactors-smrs>